Spin current, spin accumulation and spin Hall effect

2008 Sci. Technol. Adv. Mater. 9 014105

(http://iopscience.iop.org/1468-6996/9/1/014105)

IOP PUBLISHING SCIENCE AND TECHNOLOGY OF ADVANCED MATERIALS

Sci. Technol. Adv. Mater. **9** (2008) 014105 (11pp) doi:10.1088/1468-6996/9/1/014105

TOPICAL REVIEW

Spin current, spin accumulation and spin Hall effect*

Saburo Takahashi[1,2] **and Sadamichi Maekawa**[1,2,3]

[1] Institute for Materials Research, Tohoku University, Sendai 980-8577, Japan
[2] CREST, Japan Science and Technology Agency (JST), Kawaguchi 332-0012, Japan
[3] Centre for Advanced Study, Norwegian Academy of Science and Letters, Drammensveien 78, N-0271 Oslo, Norway

E-mail: takahasi@imr.tohoku.ac.jp

Received 20 September 2007
Accepted for publication 10 December 2007
Published 19 March 2008
Online at stacks.iop.org/STAM/9/014105

Abstract
Nonlocal spin transport in nanostructured devices with ferromagnetic injector (F1) and detector (F2) electrodes connected to a normal conductor (N) is studied. We reveal how the spin transport depends on interface resistance, electrode resistance, spin polarization and spin diffusion length, and obtain the conditions for efficient spin injection, spin accumulation and spin current in the device. It is demonstrated that the spin Hall effect is caused by spin–orbit scattering in nonmagnetic conductors and gives rise to the conversion between spin and charge currents in a nonlocal device. A method of evaluating spin–orbit coupling in nonmagnetic metals is proposed.

Keywords: spin polarized transport, spin injection, spin accumulation, spin current, spin detection, spin Hall effect, spin-orbit interaction, spin diffusion length

(Some figures in this article are in colour only in the electronic version.)

1. Introduction

Spin-dependent transport phenomena in magnetic nanostructures are of great interest not only in the emergence of new phenomena but also in the potential applications to spin electronic devices and information technologies [1–4]. Recent experimental and theoretical studies have demonstrated that the spin-polarized carriers injected from a ferromagnet (F) into a nonmagnetic material (N), such as a normal conducting metal, semiconductor, and superconductor, give rise to nonequilibrium spin accumulation and spin current over the spin diffusion length. Efficient spin injection, spin accumulation, spin transfer and spin detection are key factors in utilizing the spin degree of freedom as a new functionality in spin electronic devices.

In this review article, we discuss the basic theoretical aspects for spin injection, spin transport and spin detection in magnetic nanostructures containing normal conducting metals by focusing on the spin accumulation and spin current in a nonlocal spin device of F1/N/F2 structure, where F1 is a spin injector and F2 a spin detector. We derive basic spin-dependent transport equations for the electrochemical potentials (ECPs) of up- and down-spin electrons, and apply them to a structure with arbitrary electrode resistance and junction resistance ranging from a metallic contact to a tunneling regime. By analyzing the spin transport in the structure, we obtain the optimal conditions for spin accumulation and spin current. The injection of spin-polarized electrons and the detection of spin accumulation depend strongly on the nature of the junction interface (metallic contact or tunnel barrier). When a tunnel barrier is used for both junctions, the most efficient spin injection and detection are achieved.

* Invited paper.

When a metallic contact is used for the N/F2 junction, a large spin current injection into F2 is realized owing to strong spin absorption (spin sink) by F2 with a short spin diffusion length as in, for example, permalloy (Py). The latter effect is important for a nonlocal spin manipulation by nonlocal spin injection. We discuss the spin Hall effect (SHE), caused by the spin–orbit scattering of conducting electrons in nonmagnetic metals, by which the spin (charge) current is converted to charge (spin) current using a nonlocal spin device.

2. Spin injection and spin accumulation

Johnson and Silsbee [5, 6] first reported that nonequilibrium spin injected from a ferromagnet diffuses into an Al film over the spin diffusion length of the order of 1 μm (or even several hundred μm for pure Al). This rather long spin diffusion length led to the proposal of a spin injection technique using a F1/N/F2 structure (F1 is an injector and F2 a detector) [7, 8], in which the output voltage at F2 depends on the relative orientation of the magnetizations of F1 and F2. Recently, Jedema *et al* performed spin injection and detection experiments with a nonlocal measurement in a lateral structure of permalloy/copper/permalloy (Py/Cu/Py) and observed a clear spin accumulation signal at room temperature [9]. Subsequently, they measured a large spin-accumulation signal in a cobalt/aluminum/cobalt (Co/I/Al/I/Co) structure with tunnel barriers (I = Al_2O_3) [10]. Nonlocal spin injection and detection experiments have been conducted by many groups [11–25].

We consider a spin injection and detection device that consists of a nonmagnetic metal N connected to the ferromagnets of the injector F1 and detector F2, as shown in figures 1(a) and (b). F1 and F2 are ferromagnetic electrodes with width w_F and thickness d_F, and are separated by distance L. N is a normal-metal electrode with width w_N and thickness d_N. The magnetizations of F1 and F2 are aligned either parallel or antiparallel. In this device, by sending the bias current I from F1 into the left side of N, spin-polarized electrons are injected from F1 into N, and the spin accumulation is detected by F2, at distance L from F1, by measuring the voltage V_2 between F2 and N. Because of the absence of a voltage source on the right side of the device, there is no charge current in the electrodes that lie on the right side of F1. By contrast, the injected spins are diffused equally in both directions, creating spin accumulation on the right side (figure 1(c)). Accordingly, the spin and charge degrees of freedom are transported separately in the device. The advantage of the nonlocal measurement is that F2 probes only the spin degrees of freedom.

The electrical current density $\mathbf{j}_\sigma$ for spin channel σ ($\sigma = \uparrow, \downarrow$) in a conductor is driven by electric field $\mathbf{E} = -\nabla\phi$ and the gradient of carrier density n_σ:

$$\mathbf{j}_\uparrow = \sigma_\uparrow \mathbf{E} - eD_\uparrow \nabla n_\uparrow, \quad \mathbf{j}_\downarrow = \sigma_\downarrow \mathbf{E} - eD_\downarrow \nabla n_\downarrow, \qquad (1)$$

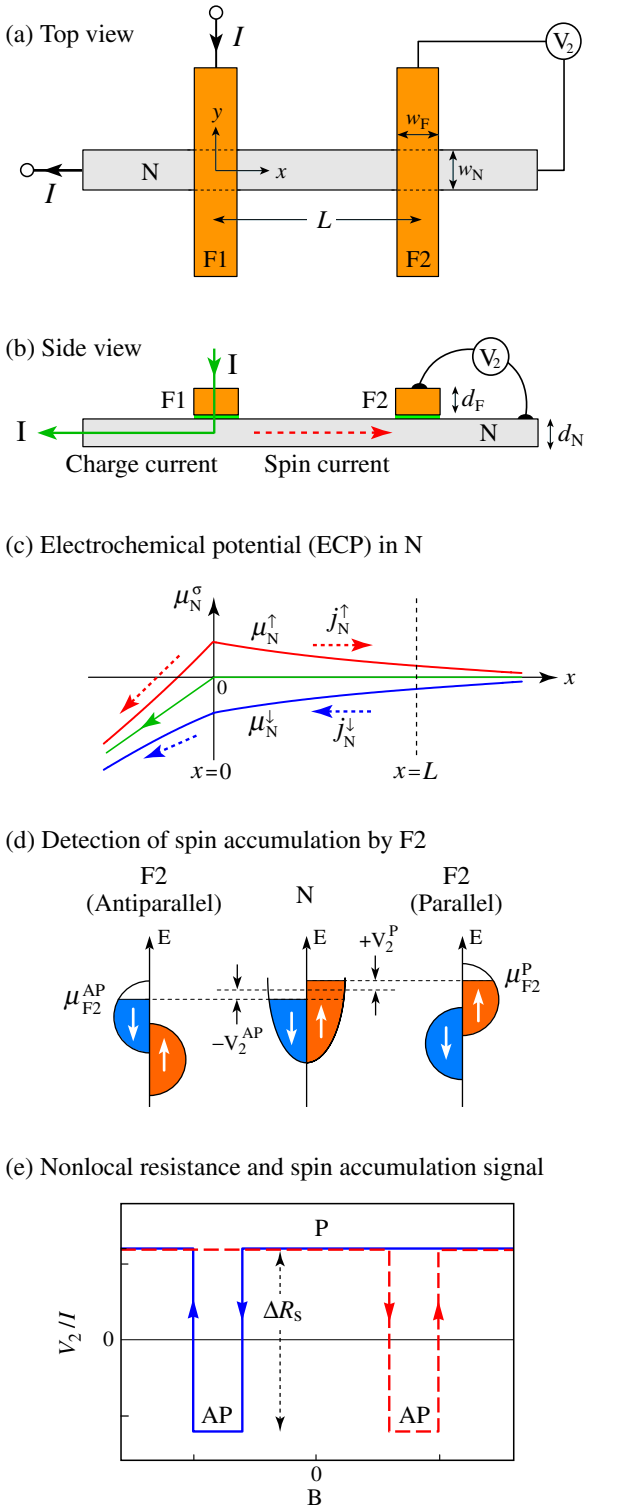

Figure 1. Nonlocal spin injection and detection device. (a) Top view. (b) Side view. Current I is sent from F1 to the left end of N. The spin accumulation at $x = L$ is proved by measuring voltage V_2 at F2. (c) Spatial variation of the ECP for up- and down-spin electrons in N. (d) Densities of states for the up- and down-spin bands in N (center) and F2 (left and right). (e) Nonlocal resistance V_2/I as a function of in-plane magnetic field B, where P and AP represent the parallel and antiparallel orientations of magnetizations in F1 and F2.

where σ_σ and D_σ are the electrical conductivity and the diffusion constant with spin σ, respectively. Using $\nabla n_\sigma = N_\sigma \nabla \varepsilon_{\rm F}^\sigma$ (N_σ is the density of states in the spin subband and $\varepsilon_{\rm F}^\sigma$ is the Fermi energy) and the Einstein relation $\sigma_\sigma = e^2 N_\sigma D_\sigma$, we have

$$\mathbf{j}_\uparrow = -(\sigma_\uparrow/e)\nabla\mu_\uparrow, \mathbf{j}_\downarrow = -(\sigma_\downarrow/e)\nabla\mu_\downarrow, \tag{2}$$

where $\mu_\sigma = \varepsilon_{\rm F}^\sigma + e\phi$ is the ECP and ϕ is the electric potential. The continuity equations for charge and spin in the steady state are

$$\nabla\cdot\left(\mathbf{j}_\uparrow + \mathbf{j}_\downarrow\right) = 0, \tag{3a}$$

$$\nabla\cdot\left(\mathbf{j}_\uparrow - \mathbf{j}_\downarrow\right) = -e\frac{\delta n_\uparrow}{\tau_{\uparrow\downarrow}} + e\frac{\delta n_\downarrow}{\tau_{\downarrow\uparrow}}, \tag{3b}$$

where $\delta n_\sigma = n_\sigma - \bar{n}_\sigma$ is the deviation from equilibrium carrier density $\bar{n}_\sigma$ with spin σ, and $\tau_{\sigma\sigma'}$ is the scattering time of an electron from spin state σ to σ'. Making use of the continuity equations and detailed balance $N_\uparrow/\tau_{\uparrow\downarrow} = N_\downarrow/\tau_{\downarrow\uparrow}$, which ensures no net spin scattering in equilibrium, we obtain the basic equations for ECP that describe the charge and spin transport [26–31]

$$\nabla^2\left(\sigma_\uparrow\mu_\uparrow + \sigma_\downarrow\mu_\downarrow\right) = 0, \tag{4a}$$

$$\nabla^2\left(\mu_\uparrow - \mu_\downarrow\right) = \frac{1}{\lambda^2}\left(\mu_\uparrow - \mu_\downarrow\right), \tag{4b}$$

where λ is the spin-diffusion length

$$\lambda = \sqrt{D\tau_{\rm sf}},$$

with spin relaxation time $\tau_{\rm sf}$ and diffusion constant D [29]:

$$\frac{1}{\tau_{\rm sf}} = \frac{1}{2}\left(\frac{1}{\tau_{\uparrow\downarrow}} + \frac{1}{\tau_{\downarrow\uparrow}}\right), \tag{5}$$

$$\frac{1}{D} = \frac{(N_\uparrow D_\downarrow^{-1} + N_\downarrow D_\uparrow^{-1})}{(N_\uparrow + N_\downarrow)}. \tag{6}$$

The physical quantities of N are spin-independent, e.g. the electrical conductivity is $\sigma_{\rm N}^\uparrow = \sigma_{\rm N}^\downarrow = \frac{1}{2}\sigma_{\rm N}$, while those of F are spin-dependent, e.g. $\sigma_{\rm F}^\uparrow \neq \sigma_{\rm F}^\downarrow$ ($\sigma_{\rm F} = \sigma_{\rm F}^\uparrow + \sigma_{\rm F}^\downarrow$). The spin-diffusion lengths of transition-metal ferromagnets are found to be $\lambda_{\rm F} \sim 5$ nm for permalloy (Py), $\lambda_{\rm F} \sim 12$ nm for CoFe, and $\lambda_{\rm F} \sim 50$ nm for Co from current-perpendicular-plane giant magnetoresistance (CPP-GMR) experiments [32], whereas those of nonmagnetic metals are $\lambda_{\rm N} \sim 1\mu$m for Cu [9, 14], and $\lambda_{\rm N} \sim 0.65\,\mu$m for Al [10]. The fact that $\lambda_{\rm F}$ of typical ferromagnets is much shorter than $\lambda_{\rm N}$ of nonmagnetic metals, such as Al or Cu, plays a crucial role in spin transport in devices with those materials.

The interfacial current across the junctions is described by using the treatment in CPP-GMR developed by Valet and Fert [27]. In the presence of spin-dependent interface resistance R_i^σ at junction i ($i = 1, 2$), the ECP changes discontinuously at the interface when the current flows across the junction. The spin-dependent interfacial current I_1^σ (I_2^σ) from F1 (F2) to N is given by the ECP difference at the interface [27–29]: $I_1^\sigma = (\mu_{\rm F1}^\sigma - \mu_{\rm N}^\sigma)/(eR_1^\sigma)$ and $I_2^\sigma = (\mu_{\rm F2}^\sigma - \mu_{\rm N}^\sigma)/(eR_2^\sigma)$, where the distribution of the current is assumed to be uniform over the interface. The total charge and spin currents across the ith interface are $I_i = I_i^\uparrow + I_i^\downarrow$ and $I_i^{\rm s} = I_i^\uparrow - I_i^\downarrow$. The above interfacial currents are applicable to tunnel junctions as well as to transparent metallic contacts. In a transparent metallic contact ($R_i^\sigma \to 0$), the continuity of ECPs at the interface acts as a strong constraint for spin accumulation on the N side, because the spin accumulation on F is very small owing to the short spin diffusion length. In a tunnel junction, spin accumulation on the N side is free from the constraint owing to a large discontinuous change in ECPs at the junction.

In a real device, the distribution of the current across the interface depends on the relative magnitude of the interface resistance to the electrode resistance [33]. When the interface resistance is much larger than the electrode resistance as in tunnel junctions, the current distribution is uniform in the contact area [34], which validates the assumption of uniform interface current. However, when the interface resistance is comparable to or smaller than the electrode resistance as in metallic contact junctions, the interface current has inhomogeneous distribution with a high current density around a corner of the contact [17, 35]. In this case, the effective contact area through which most of the current passes is smaller than the actual contact area $A_{\rm J} = w_{\rm N}w_{\rm F}$ of the junctions.

When current I is sent from F1 to the left side of N ($I_1 = I$) the solution of equations (4*a*) and (4b) takes the form

$$\mu_{\rm N}^\sigma = \bar{\mu}_{\rm N} + \sigma\left(a_1 {\rm e}^{-|x|/\lambda_{\rm N}} - a_2 {\rm e}^{-|x-L|/\lambda_{\rm N}}\right), \tag{7}$$

where the first term describes the charge transport and is $\bar{\mu}_{\rm N} = -[eI/(\sigma_{\rm N}A_{\rm N})]x$ ($A_{\rm N} = d_{\rm N}w_{\rm N}$) for $x < 0$ and $\bar{\mu}_{\rm N} = 0$ (ground level of ECP) for $x > 0$, and the second term is the shift in ECP of up-spin ($\sigma = +$) and down-spin ($\sigma = -$) electrons, where the a_1 term represents the spin accumulation due to spin injection from F1, while the a_2 term is the spin depletion due to spin leakage into F2. Note that the pure spin current flows in the region of $x > 0$, i.e. the charge current ($j_{\rm N} = j_{\rm N}^\uparrow + j_{\rm N}^\downarrow$) is absent and only the spin current ($j_{\rm N}^{\rm s} = j_{\rm N}^\uparrow - j_{\rm N}^\downarrow$) flows (figure 1(c)).

In the F1 and F2 electrodes, the thicknesses are much larger than the spin diffusion length ($d_{\rm F} \gg \lambda_{\rm F}$), as in the case of Py or CoFe, so that the solutions close to the interfaces may take the forms of vertical transport along the z-direction: $\mu_{\rm F1}^\sigma = \bar{\mu}_{\rm F1} + \sigma(b_1/\sigma_{\rm F}^\sigma){\rm e}^{-z/\lambda_{\rm F}}$ and $\mu_{\rm F2}^\sigma = \bar{\mu}_{\rm F2} - \sigma(b_2/\sigma_{\rm F}^\sigma){\rm e}^{-z/\lambda_{\rm F}}$, where $\bar{\mu}_{\rm F1} = -[eI/(\sigma_{\rm F}A_{\rm J})]z + eV_1$ describes the charge current flow in F1, $\bar{\mu}_{\rm F2} = eV_2$ has a constant potential with no charge current in F2, and V_1 and V_2 are the voltage drops across junctions 1 and 2.

Making use of the matching conditions that the spin current is continuous at the interfaces of junctions 1 and 2, the coefficients a_i, b_i, and V_i in ECPs are determined. The detected voltages, $V_2^{\rm P}$ and $V_2^{\rm AP}$, in the parallel (P) and antiparallel (AP) alignments of magnetizations (figure 1(d)) are used to calculate the spin accumulation

signal $\Delta R_s = (V_2^P - V_2^{AP})/I$, yielding [30]

$$\Delta R_s = R_N \frac{(2P_1 r_1 + 2p_F r_F)(2P_2 r_2 + 2p_F r_F)\, e^{-L/\lambda_N}}{(1 + 2r_1 + 2r_F)(1 + 2r_2 + 2r_F) - e^{-2L/\lambda_N}}, \quad (8)$$

with the normalized resistances

$$r_i = \frac{1}{(1 - P_i^2)} \frac{R_i}{R_N}, \qquad r_F = \frac{1}{(1 - p_F^2)} \frac{R_F}{R_N}, \quad (9)$$

where R_i $(1/R_i = 1/R_i^{\uparrow} + 1/R_i^{\downarrow})$ is the interface resistance of junction i, R_N and R_F are the resistances of the N and F electrodes with the lengths of λ_N and λ_F and are called spin resistances:

$$R_N = (\rho_N \lambda_N)/A_N, \qquad R_N = (\rho_F \lambda_F)/A_J, \quad (10)$$

with the resistivity ρ_N and the cross-sectional area $A_N = w_N d_N$ of N, the resistivity ρ_F of F and the contact area $A_J = w_N w_F$ of the junctions. P_i is the interfacial current spin polarization and p_F the spin polarization of F1 and F2:

$$P_i = \left|R_i^{\uparrow} - R_i^{\downarrow}\right| / \left(R_i^{\uparrow} + R_i^{\downarrow}\right), \quad (11)$$

$$p_F = \left|\rho_F^{\uparrow} - \rho_F^{\downarrow}\right| / \left(\rho_F^{\uparrow} + \rho_F^{\downarrow}\right), \quad (12)$$

where $\rho_F^{\sigma} = 1/\sigma_F^{\sigma}$ is the spin-dependent electrical resistivity of F. In metallic contact junctions, the spin polarizations (P_i and p_F), are in the range of around 50–70%, as determined from GMR experiments [32] and point-contact Andreev-reflection experiments [36], whereas in tunnel junctions, P_i is in the range of around 30–55% with alumina (Al_2O_3) tunnel barriers [37–39], and ~85% with MgO barriers [40, 41], as determined from superconducting tunneling spectroscopy experiments.

The spin accumulation signal ΔR_s strongly depends on the relative magnitude between the junction resistances (R_1, R_2) and the electrode resistances (R_N, and R_N). Since R_N is much smaller than R_N ($R_N \gg R_N$), as in a device with Cu and Py, we have the following cases. When both junctions are tunnel junctions ($R_1, R_2 \gg R_N \gg R_N$) [8, 10],

$$\Delta R_s / R_N = P_T^2 e^{-L/\lambda_N}, \quad (13)$$

where P_T is the tunnel spin polarization. When junction 1 is a tunnel junction and junction 2 is a transparent metallic contact ($R_1 \gg R_N \gg R_N \gg R_2$) [30],

$$\Delta R_s / R_N = \frac{2p_F P_T}{1 - p_F^2} \left(\frac{R_N}{R_N}\right) e^{-L/\lambda_N}. \quad (14)$$

When both junctions are transparent metallic contacts ($R_N \gg R_N \gg R_1, R_2$) [9, 28, 29, 42],

$$\Delta Rs / R_N = \frac{2p_F^2}{(1 - p_F^2)^2} \left(\frac{R_N}{R_N}\right)^2 \frac{1}{\sinh(L/\lambda_N)}. \quad (15)$$

Note that ΔR_s in the above limiting cases is independent of R_i.

Figure 2(a) shows the spin accumulation signal ΔR_s for $R_N/R_N = 0.01$ [9], $p_F = 0.7$, and $P_1 = P_2 = 0.4$. We see that ΔR_s increases by one order of magnitude by replacing a metallic contact with a tunnel barrier, since the resistance mismatch, which is represented by $(R_F/R_N) \ll 1$, is removed by replacing a metallic contact with a tunnel junction. Note that the mismatch originates from a large difference in the spin diffusion lengths between N and F ($\lambda_F \ll \lambda_N$). When a nonmagnetic semiconductor is used for N, the resistance mismatch arises from the resistivity mismatch ($\rho_N \gg \rho_F$) [42–44].

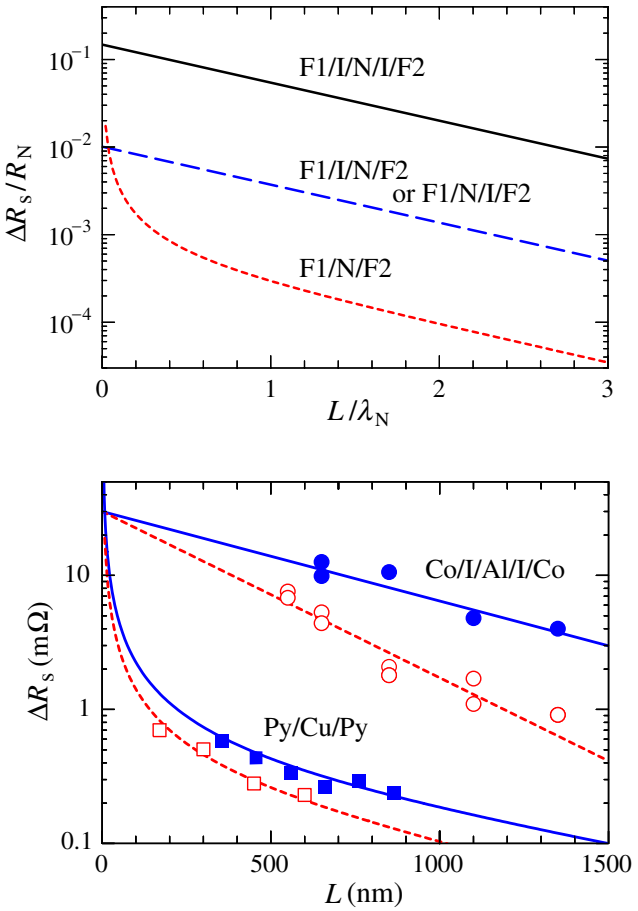

Figure 2. (a) Spin accumulation signal ΔR_s as a function of distance L between F1 and F2. (b) Spin accumulation signal ΔR_s as a function of distance L in a tunnel device and a metallic contact device. The symbols (●, ○) are the experimental data of Co/I/Al/I/Co [10], and (□, ■) are those of Py/Cu/Py [46, 47], where (●, ■) and (○, □) were measured at 4.2 K and at room temperature, respectively.

A controversial discussion has been raised on whether the contacts in the metallic Py/Cu/Py structure [9] are really transparent junctions ($R_i/R_F \ll 1$) or, rather, tunnel-like junctions ($R_i/R_N \gg 1$) [45]. If one uses the experimental values ($R_i A_J \sim 2 \times 10^{-12}\ \Omega\text{cm}^2$, $\lambda_F \sim 5$ nm [32], $\rho_F \sim 10^{-5}\ \Omega$cm), one obtains $R_i/R_F \sim 0.4$, indicating that Py/Cu/Py lies in the transparent regime, so that equation (15) may be used to analyze the experimental data.

Figure 2(b) shows the experimental data of ΔR_s as a function of distance L in Co/I/Al/I/Co [10] and Py/Cu/Py [46, 47]. In the tunnel device of Co/I/Al/I/Co (I = Al_2O_3), fitting equation (13) to the data of Jedema *et al* [10] yields $\lambda_N = 650$ nm at 4.2 K, $\lambda_N = 350$ nm at 293 K, $P_T = 0.1$

and $R_N = 3\,\Omega$.[1] The relation $\lambda_N^2 = D\tau_{sf}$ with $\lambda_N = 650\,nm$ and $D = 1/[2e^2N(0)\rho_N] \sim 40\,cm^2\,s^{-1}$ leads to $\tau_{sf} = 100\,ps$ at 4.2 K, which is consistent with the value of the spin–orbit parameter $b = \hbar/(3\tau_{sf}\Delta_{Al}) \sim 0.01$ obtained by superconducting tunneling spectroscopy [39, 40]. In the metallic contact device of Py/Cu/Py, fitting equation (15) to the data of Garzon [46] yields $\lambda_N = 920\,nm$, $R_N = 5\,\Omega$,[2] and $[p_F/(1-p_F^2)]R_F = 24\,m\Omega$ at 4.2 K, and fitting equation (15) to the data of Kimura *et al* [47] yields $\lambda_N = 700\,nm$, $R_N = 2\,\Omega$,[3] and $[p_F/(1-p_F^2)]R_F = 14\,m\Omega$ at 293 K.

In the tunneling regime, the spin splitting of ECP at position x in N is given by

$$2\delta\mu_N(x) = P_T e R_N I e^{-|x|/\lambda_N}. \quad (16)$$

For a device with $P_T \sim 0.1$, $R_N = 3\,\Omega$ and $I = 100\,\mu A$ [10], the value of $\delta\mu_N(x)$ at $x = 0$ is about $\sim 15\,\mu V$, which is much smaller than the superconducting gap $\Delta \sim 200\,\mu eV$ of Al films. In a device with a SC (Al), a large enhancement of the spin accumulation signal ΔR_s in the superconducting state has been predicted [30] and observed experimentally [48, 49].

It is noteworthy that when F1 and F2 are both half-metallic ferromagnets ($p_F = 1, r_F \gg 1$), we have the largest signal

$$\Delta R_s \approx R_N e^{-L/\lambda_N}, \quad (17)$$

without tunnel barriers, which is the advantage of using a half-metallic ferromagnet with 100% spin polarization.

3. Nonlocal spin-current injection and manipulation

We next investigate how the spin current flows through the nonlocal structure, particularly the spin current across the N/F2 interface (figure 3(a)), because of an interest in magnetization switching [50–52] caused by pure spin-current injection in nonlocal devices [53–55].

The magnitude and distribution of the spin accumulation and spin current in a nonlocal device is strongly influenced by the relative magnitudes of the interface resistances (R_i) and the electrode spin resistances (R_F, R_N). Figure 3(b) shows the spatial variation of spin accumulation $\delta\mu_N$ in the N electrode in the F1/I/N/F2 structure. The dashed curve indicates $\delta\mu_N$ in the absence of F2. When F2 is in contact with N at the position of $L/\lambda_N = 0.5$, the spin accumulation is strongly suppressed by F2 with short R_F, leaving little spin accumulation on the right side of F2. This behavior has been observed in a nonlocal device with three Py electrodes [13, 14]. We also note that the slope of the curve between F1 and F2 ($0 < x < L$) becomes steeper than that of the dashed curve, indicating that the spin currents I_N^s between F1 and F2 become larger than that in the absence of F2, as seen in figure 3(c). The large discontinuous drop of I_N^s at $x = L$ is caused by strong absorption of the spin current by F2, indicating that most of the spin current flows out of N into F2 through the N/F2 interface. In the N region on the right side of F2 ($x > L$), the spin current is very small. This implies that F2 with a very low R_F, such as Py and CoFe, and with a metallic contact with N acts as a strong spin absorber (an ideal spin sink).

[1] $\rho_N = 6\,\mu\Omega cm$, $\lambda_N = 0.65\,\mu m$ and $A_N = 250 \times 50\,nm^2$ for Al [10]
[2] $\rho_N = 3\,\mu\Omega cm$, $\lambda_N = 0.92\,\mu m$, and $A_N = 125 \times 45\,nm^2$ for Cu [46].
[3] $\rho_N = 2.0\,\mu\Omega cm$ $\lambda_N = 0.7\,\mu m$, and $A_N = 100 \times 80\,nm^2$ for Cu [47].

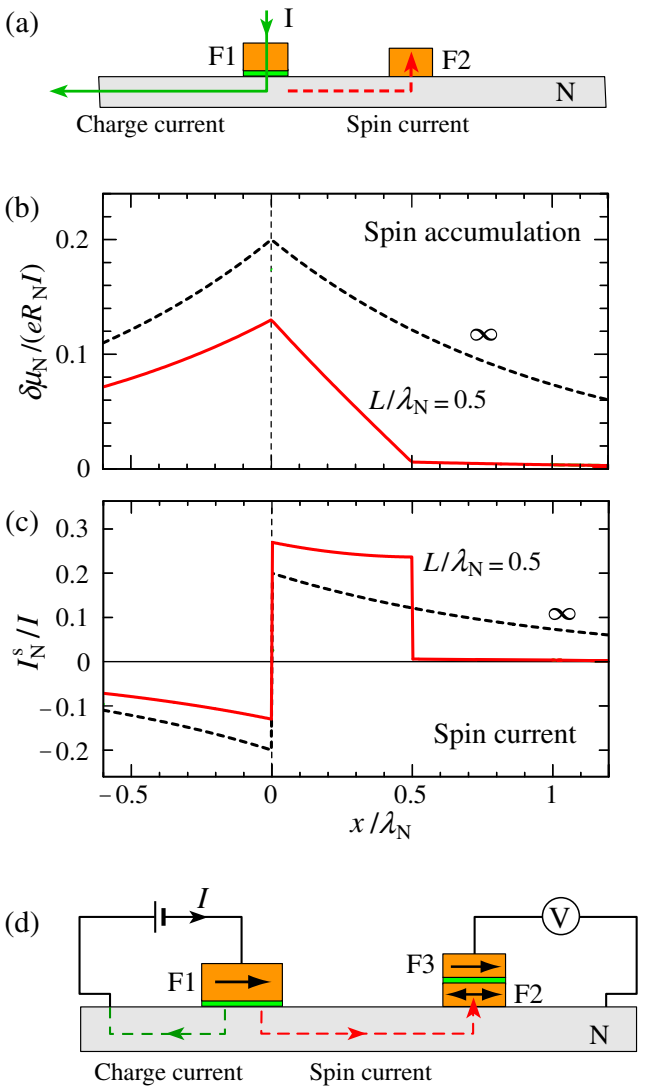

Figure 3. (a) Nonlocal spin current injection device of F1/I/N/F2, where junction 1 is a tunnel junction and second 2 is a metallic contact. Spatial variations of (b) spin accumulation $\delta\mu_N$ and (c) spin current I_N^s in N for $L/\lambda_N = 0.5$ and ∞. The parameter values are the same as those in figure 2. The discontinuous change of spin current at $L/\lambda_N = 0.5$ indicates that most of the spin current flows out of N through the N/F2 interface. (d) Spin switching device utilizing nonlocal spin current injection [53]. The magnetization direction in F2 is detected by F3.

The spin current I_2^s across the N/F2 interface is calculated as [30, 54]

$$I_2^s = \frac{2\,(P_1 r_1 + p_F r_F)\,e^{-L/\lambda_N} I}{(1+2r_1+2r_F)\,(1+2r_2+2r_F) - e^{-2L/\lambda_N}}, \quad (18)$$

which leads to the spin-current injection from N into F2 being the largest when the first junction is a tunnel junction ($r_1 \gg 1$), the second junction is a metallic contact ($r_2 \ll 1$), and F2 is a strong spin absorber ($R_{F2} \ll R_N$), such as Py or CoFe, yielding the spin-current injected nonlocally into F2 as

$$I_2^s \approx P_T I e^{-L/\lambda_N}. \quad (19)$$

When a small F2 island is placed on N with the contact area of $(100\,nm)^2$ at distance $L \sim \lambda_N$, the injected spin current

density into F2 becomes of the order of $I_2^s \sim 10^6\,\mathrm{A\,cm^{-2}}$ or more for $I = 1\,\mathrm{mA}$ and $P_\mathrm{T} = 0.3$, suggesting that a large spin current injection is achieved, and hence, the spin-angular momentum is efficiently transferred from F1 to a small F2. This result provides a method for manipulating the orientation of magnetization due to spin transfer torque in nonlocal spin devices [55].

4. SHE

The anomalous Hall effect (AHE) originates from the relativistic interaction between the spin and orbital motion of electrons (spin–orbit interaction) in metals or semiconductors. Conduction electrons are scattered by local potentials created by impurities or defects in a crystal. The spin–orbit interaction at local potentials causes a spin-asymmetric scattering of conduction electrons [56]. In ferromagnetic materials, up-spin (majority) electrons are scattered preferentially in one direction and down-spin (minority) electrons in the opposite direction, resulting in a transverse current in the direction perpendicular to both the applied electric field and the magnetization directions.

Nonlocal spin injection in nanostructured devices provides a new opportunity for observing AHE in *nonmagnetic* conductors, which is called the SHE. If spin-polarized electrons flow in a nonmagnetic electrode (N), these electrons are deflected by spin–orbit scattering to induce spin and charge Hall currents in the transverse direction and accumulate spin and charge at the edges of N [57–62]. Using nonlocal spin injection and detection devices, the following two kinds of SHE are observable. When a spin current without accompanying charge current (pure spin current) is created in N via nonlocal spin injection, the up- and down-spin currents, which flow in opposite directions, are deflected in the same direction to induce a charge current in the transverse direction and the charge accumulates on the edges of N. Inversely, when an unpolarized charge current flows in N as a result of an applied electric field, the up- and down-spin currents, which flow in the same direction, are deflected in the opposite direction to induce a spin current in the transverse direction, and the spin accumulates near the edges of N. As a consequence, the spin (charge) degrees of freedom are converted to charge (spin) degrees of freedom because of spin–orbit scattering in nonmagnetic conductors. Recently, SHE has been observed using nonlocal spin injection in metal-based nanostructured devices [63–67], which paves the way for future spin electronic applications. In addition to these *extrinsic* SHEs, *intrinsic* SHEs have been intensively studied in semiconductors which do not require impurities or defects [68–73].

In the following, we consider the effect of spin–orbit scattering on the spin and charge transports in nonmagnetic metals (N) such as Cu, Al and Ag, and discuss SHE by taking into account the *side jump* (SJ) and *skew scattering* (SS) mechanisms [56, 74–76], and derive formulae for the SHE induced by spin–orbit scattering in nonmagnetic metals [60].

4.1. Basic formulation

The spin–orbit interaction in the presence of nonmagnetic impurities in a metal is derived as follows [77]. The impurity potential $V(\mathbf{r})$ gives rise to an additional electric field $\mathbf{E} = -(1/e)\nabla V(\mathbf{r})$. When an electron passes through the field with velocity $\hat{\mathbf{p}}/m = (\hbar/i)\nabla/m$, the electron feels an effective magnetic field $\mathbf{B}_\mathrm{eff} = -(1/mc)\hat{\mathbf{p}} \times \mathbf{E}$, which leads to the spin–orbit coupling $V_\mathrm{so} = -\mu_\mathrm{B}\boldsymbol{\sigma}\cdot\mathbf{B}_\mathrm{eff} = \eta_\mathrm{so}\boldsymbol{\sigma}\cdot[\nabla V(\mathbf{r}) \times \nabla/i]$, where $\boldsymbol{\sigma}$ is the Pauli spin operator and η_so is the spin–orbit coupling parameter. The total impurity potential $U(\mathbf{r})$ is the sum of the ordinary impurity potential and the spin–orbit potential: $U(\mathbf{r}) = V(\mathbf{r}) + V_\mathrm{so}(\mathbf{r})$.

In the presence of the impurity potential $U(\mathbf{r})$, the scattering of conduction electrons between states $|\mathbf{k}\sigma\rangle$ with momentum $\mathbf{k}$ and spin σ is described by the scattering amplitude $U^{\sigma'\sigma}_{\mathbf{k}'\mathbf{k}} = \langle\mathbf{k}'\sigma'|U|\mathbf{k}\sigma\rangle$ given by

$$U^{\sigma'\sigma}_{\mathbf{k}'\mathbf{k}} = V_\mathrm{imp}\left[\delta_{\sigma'\sigma} + \mathrm{i}\eta_\mathrm{so}\boldsymbol{\sigma}_{\sigma'\sigma}\cdot(\mathbf{k}\times\mathbf{k}')\right]\sum_i \mathrm{e}^{\mathrm{i}(\mathbf{k}-\mathbf{k}')\cdot\mathbf{r}_i}, \quad (20)$$

where $\boldsymbol{\sigma}$ is the Pauli matrix and $V_\mathrm{imp}\sum_i \mathrm{e}^{\mathrm{i}(\mathbf{k}-\mathbf{k}')\cdot\mathbf{r}_i}$ represents the matrix elements of the weak δ-function potential $V(\mathbf{r}) \approx V_\mathrm{imp}\sum_i \delta(\mathbf{r}-\mathbf{r}_i)$ for impurities at position $\mathbf{r}_i$.

The velocity $\mathbf{v}^\sigma_\mathbf{k}$ of an electron in the presence of spin–orbit potential is calculated as follows. By taking the matrix element $\mathbf{v}^\sigma_\mathbf{k} = \langle\mathbf{k}^+\sigma|\hat{\mathbf{v}}|\mathbf{k}^+\sigma\rangle$ of the velocity operator $\hat{\mathbf{v}} = \mathrm{d}\mathbf{r}/\mathrm{d}t$ [78] between the scattering states,

$$|\mathbf{k}^+\sigma\rangle = |\mathbf{k}\sigma\rangle + \sum_{\mathbf{k}'}|\mathbf{k}'\sigma\rangle\frac{V_\mathrm{imp}\sum_i \mathrm{e}^{\mathrm{i}(\mathbf{k}-\mathbf{k}')\cdot\mathbf{r}_i}}{\xi_\mathbf{k} - \xi_{\mathbf{k}'} + i\delta}, \quad (21)$$

where $|\mathbf{k}\sigma\rangle$ is the one-electron state with momentum $\mathbf{k}$, spin σ, and kinetic energy $\xi_\mathbf{k} = (\hbar k)^2/2m - \varepsilon_\mathrm{F}$, we obtain

$$\mathbf{v}^\sigma_\mathbf{k} = \hbar\mathbf{k}/m + \boldsymbol{\omega}^\sigma_\mathbf{k} \quad (22)$$

with the usual velocity $\hbar\mathbf{k}/m$ and *anomalous velocity*

$$\boldsymbol{\omega}^\sigma_\mathbf{k} = \alpha^\mathrm{SJ}_\mathrm{H}\left(\boldsymbol{\sigma}_{\sigma\sigma}\times\hbar\mathbf{k}/m\right), \quad (23)$$

where $\alpha^\mathrm{SJ}_\mathrm{H}$ is the dimensionless coupling parameter of the side jump

$$\alpha^\mathrm{SJ}_\mathrm{H} = \frac{m\eta_\mathrm{so}}{\hbar\tau^0_\mathrm{tr}} = \frac{\hbar\bar{\eta}_\mathrm{so}}{2\varepsilon_\mathrm{F}\tau^0_\mathrm{tr}} = \frac{\bar{\eta}_\mathrm{so}}{k_\mathrm{F}l} \quad (24)$$

with the scattering time $\tau^0_\mathrm{tr} = 1/[(2\pi/\hbar)n_\mathrm{imp}N(0)V^2_\mathrm{imp}]$, the impurity concentration n_imp, the dimensionless spin–orbit coupling parameter $\bar{\eta}_\mathrm{so} = k^2_\mathrm{F}\eta_\mathrm{so}$, the Fermi momentum k_F, and the mean-free path $l = v_\mathrm{F}\tau^0_\mathrm{tr}$.

Introducing the current operator for conduction electrons with spin σ,

$$\hat{\mathbf{J}}_\sigma = e\sum_\mathbf{k}\left(\hbar\mathbf{k}/m + \boldsymbol{\omega}^\sigma_\mathbf{k}\right)a^\dagger_{\mathbf{k}\sigma}a_{\mathbf{k}\sigma} \quad (25)$$

($e = -|e|$ is the electronic charge), the total charge current $\mathbf{J}_\mathrm{q} = \mathbf{J}_\uparrow + \mathbf{J}_\downarrow$ and the total spin current $\mathbf{J}_\mathrm{s} = \mathbf{J}_\uparrow - \mathbf{J}_\downarrow$ are expressed as

$$\mathbf{J}_\mathrm{q} = \mathbf{J}'_\mathrm{q} + \alpha^\mathrm{SJ}_\mathrm{H}\left[\hat{\mathbf{z}}\times\mathbf{J}'_\mathrm{s}\right], \quad (26)$$

$$\mathbf{J}_s = \mathbf{J}'_s + \alpha_H^{SJ}\left[\hat{\mathbf{z}} \times \mathbf{J}'_q\right], \tag{27}$$

where

$$\mathbf{J}'_q = e\sum_{\mathbf{k}} \frac{\hbar\mathbf{k}}{m}\left(f_{\mathbf{k}\uparrow} + f_{\mathbf{k}\downarrow}\right), \tag{28}$$

$$\mathbf{J}'_s = e\sum_{\mathbf{k}} \frac{\hbar\mathbf{k}}{m}\left(f_{\mathbf{k}\uparrow} - f_{\mathbf{k}\downarrow}\right), \tag{29}$$

and $f_{\mathbf{k}\sigma} = \langle a^\dagger_{\mathbf{k}\sigma} a_{\mathbf{k}\sigma}\rangle$ is the distribution function of an electron with energy $\xi_{\mathbf{k}}$ and spin σ. The second terms in equations (26) and (27) are the charge and spin Hall currents induced by side jump. In addition to the side jump contribution, there is the skew scattering contribution which originates from the anisotropic scattering due to the spin–orbit interaction and modifies the distribution function.

The distribution function $f_{\mathbf{k}\sigma}$ is calculated based on the Boltzmann transport equation in the steady state,

$$\mathbf{v}_{\mathbf{k}} \cdot \nabla f_{\mathbf{k}\sigma} + \frac{e\mathbf{E}}{\hbar} \cdot \nabla_{\mathbf{k}} f_{\mathbf{k}\sigma} = \left(\frac{\partial f_{\mathbf{k}\sigma}}{\partial t}\right)_{\text{scatt}}, \tag{30}$$

where $\mathbf{v}_{\mathbf{k}} = \hbar\mathbf{k}/m$, $\mathbf{E}$ is the external electric field, and the collision term due to impurity scattering in the rhs is written as

$$\begin{aligned}\left(\frac{\partial f_{\mathbf{k}\sigma}}{\partial t}\right)_{\text{scatt}} &= \sum_{\mathbf{k}'\sigma'}\left[P^{\sigma\sigma'}_{\mathbf{k}\mathbf{k}'} f_{\mathbf{k}'\sigma'} - P^{\sigma'\sigma}_{\mathbf{k}'\mathbf{k}} f_{\mathbf{k}\sigma}\right] \\ &= \sum_{\mathbf{k}'\sigma'} P^{\sigma'\sigma\,(1)}_{\mathbf{k}'\mathbf{k}}\left(f_{\mathbf{k}'\sigma'} - f_{\mathbf{k}\sigma}\right) \\ &\quad + \sum_{\mathbf{k}'\sigma'} P^{\sigma'\sigma\,(2)}_{\mathbf{k}'\mathbf{k}}\left(f_{\mathbf{k}'\sigma} + f_{\mathbf{k}\sigma}\right),\end{aligned} \tag{31}$$

where the first term in the brackets is the scattering-in term ($\mathbf{k}'\sigma' \to \mathbf{k}\sigma$) and the second term is the scattering-out term ($\mathbf{k}\sigma \to \mathbf{k}'\sigma'$), $P^{\sigma'\sigma}_{\mathbf{k}'\mathbf{k}}$ is the scattering probability from state $|\mathbf{k}\sigma\rangle$ to state $|\mathbf{k}'\sigma'\rangle$ and is calculated by $P^{\sigma'\sigma}_{\mathbf{k}'\mathbf{k}} = (2\pi/\hbar)n_{\text{imp}}|\langle\mathbf{k}'\sigma'|\hat{T}|\mathbf{k}\sigma\rangle|^2\delta(\xi_{\mathbf{k}} - \xi_{\mathbf{k}'})$ using the $\hat{T}$-matrix, and $P^{\sigma'\sigma\,(1)}_{\mathbf{k}'\mathbf{k}}$ and $P^{\sigma'\sigma\,(2)}_{\mathbf{k}'\mathbf{k}}$ are, respectively, the first-order symmetric and the second-order asymmetric contributions:

$$\begin{aligned}P^{\sigma'\sigma\,(1)}_{\mathbf{k}'\mathbf{k}} &= \frac{2\pi}{\hbar} n_{\text{imp}} V^2_{\text{imp}} \times \left(\delta_{\sigma\sigma'} + \left|\eta_{\text{so}}(\mathbf{k}'\times\mathbf{k})\cdot\boldsymbol{\sigma}_{\sigma\sigma'}\right|^2\right) \\ &\quad \times \delta(\xi_{\mathbf{k}'} - \xi_{\mathbf{k}}),\end{aligned} \tag{32}$$

$$\begin{aligned}P^{\sigma'\sigma\,(2)}_{\mathbf{k}'\mathbf{k}} &= \frac{(2\pi)^2}{\hbar} n_{\text{imp}} V^3_{\text{imp}} N(0) \times \left[\eta_{\text{so}}(\mathbf{k}'\times\mathbf{k})\cdot\boldsymbol{\sigma}_{\sigma\sigma}\right] \\ &\quad \times \delta_{\sigma\sigma'}\delta(\xi_{\mathbf{k}'} - \xi_{\mathbf{k}}),\end{aligned} \tag{33}$$

In solving the Boltzmann transport equation, it is convenient to separate $f_{\mathbf{k}\sigma}$ into three parts [79] as

$$f_{\mathbf{k}\sigma} = f^0_{k\sigma} + g^{(1)}_{\mathbf{k}\sigma} + g^{(2)}_{\mathbf{k}\sigma}, \tag{34}$$

where $f^0_{k\sigma}$ is a nondirectional distribution function defined by the average of $f_{\mathbf{k}\sigma}$ with respect to the solid angle $\Omega_{\mathbf{k}}$ of $\mathbf{k}$:

$$f^0_{k\sigma} = \int f_{\mathbf{k}\sigma}\frac{\mathrm{d}\Omega_{\mathbf{k}}}{(4\pi)},$$

and $g^{(1)}_{\mathbf{k}\sigma}$ and $g^{(2)}_{\mathbf{k}\sigma}$ are directional distribution functions, i.e. $\int g^{(i)}_{\mathbf{k}\sigma}\mathrm{d}\Omega_{\mathbf{k}} = 0$, and are associated with the first-order and the second-order transitions, respectively.

The first term in equation (31) is written as

$$\sum_{\mathbf{k}'\sigma'}\left[P^{\sigma\sigma'\,(1)}_{\mathbf{k}\mathbf{k}'} f_{\mathbf{k}'\sigma'} - P^{\sigma'\sigma\,(1)}_{\mathbf{k}'\mathbf{k}} f_{\mathbf{k}\sigma}\right] = -\frac{g^{(1)}_{\mathbf{k}\sigma}}{\tau_{\text{tr}}} - \frac{f^0_{k\sigma} - f^0_{k-\sigma}}{\tau_{\text{sf}}(\theta)}, \tag{35}$$

where τ_{tr} is the transport relaxation time and $\tau_{\text{sf}}(\theta)$ is the spin–flip relaxation time,

$$1/\tau_{\text{tr}}(\theta) = \sum_{\mathbf{k}'\sigma'} P^{\sigma\sigma'\,(1)}_{\mathbf{k}\mathbf{k}'} = \frac{1}{\tau^0_{\text{tr}}}\left(1 + 2\bar{\eta}^2_{\text{so}}/3\right), \tag{36a}$$

$$1/\tau_{\text{sf}}(\theta) = \sum_{\mathbf{k}'} P^{\uparrow\downarrow\,(1)}_{\mathbf{k}\mathbf{k}'} = \frac{\bar{\eta}_{\text{so}}{}^2}{3\tau^0_{\text{tr}}}\left(1 + \cos^2\theta\right), \tag{36b}$$

with the angle θ between $\mathbf{k}$ and the x-axis. Then, the Boltzmann equation (30) with the collision term (35) is [59, 80]

$$\mathbf{v}_{\mathbf{k}} \cdot \frac{\partial f_{\mathbf{k}\sigma}}{\partial \mathbf{r}} + \frac{e\mathbf{E}}{\hbar} \cdot \frac{\partial f_{\mathbf{k}\sigma}}{\partial \mathbf{k}} = -\frac{g^{(1)}_{\mathbf{k}\sigma}}{\tau_{\text{tr}}} - \frac{f^0_{k\sigma} - f^0_{k-\sigma}}{\tau_{\text{sf}}(\theta)}, \tag{37}$$

where the first term in the rhs describes the momentum relaxation due to impurity scattering and the second term the spin relaxation due to spin–flip scattering. Since $\tau_{\text{tr}} \ll \tau_{\text{sf}}$, the momentum relaxation occurs first, followed by slow spin relaxation.

The first-order solution due to momentum relaxation is obtained as

$$g^{(1)}_{\mathbf{k}\sigma} \approx -\tau_{\text{tr}}\left(\mathbf{v}_{\mathbf{k}} \cdot \nabla + \frac{e\mathbf{E}}{\hbar} \cdot \nabla_{\mathbf{k}}\right) f^0_{k\sigma}. \tag{38}$$

The distribution function $f^0_{k\sigma}$ is a local equilibrium one with Fermi energy $\varepsilon^\sigma_{\text{F}}(\mathbf{r}) = \varepsilon_{\text{F}} + \sigma\delta\varepsilon_{\text{F}}(\mathbf{r})$ shifted by $\sigma\delta\varepsilon_{\text{F}}(\mathbf{r})$ from the global equilibrium, and may be expanded as

$$f^0_{k\sigma} \approx f_0(\xi_{\mathbf{k}}) - \sigma\frac{\partial f_0(\xi_{\mathbf{k}})}{\partial \xi_{\mathbf{k}}}\delta E_{\text{F}}(\mathbf{r}), \tag{39}$$

where $f_0(\xi_{\mathbf{k}})$ is the Fermi distribution function. Therefore, equation (38) becomes

$$g^{(1)}_{\mathbf{k}\sigma} \approx \tau_{\text{tr}}\frac{\partial f_0(\xi_{\mathbf{k}})}{\partial \xi_{\mathbf{k}}}\mathbf{v}_{\mathbf{k}} \cdot \nabla\mu^\sigma_{\text{N}}(\mathbf{r}), \tag{40}$$

with the electrochemical potential (ECP) $\mu^\sigma_{\text{N}}(\mathbf{r}) = \varepsilon_{\text{F}} + e\phi + \sigma\delta\varepsilon_{\text{F}}$ and the electric potential ϕ ($\mathbf{E} = -\nabla\phi$).

The spin–flip scattering by the spin–orbit interaction causes a slow relaxation for spin accumulation $(\mu_N^{\uparrow} - \mu_N^{\downarrow}) = 2\delta\mu_N$. By substituting equations (34), (39) and (40) into the Boltzmann equation (37) and summing over $\mathbf{k}$, one obtains the spin diffusion equation

$$\nabla^2 \delta\mu_N = \frac{1}{\lambda_N^2}\delta\mu_N \tag{41}$$

with $\lambda_N = \sqrt{D\tau_{sf}}$, $D = (1/3)\tau_{tr}v_F^2$, and $\tau_{sf}^{-1} = \langle\tau_{sf}^{-1}(\theta)\rangle_{av} = 4\bar{\eta}_{so}^2/(9\tau_{tr}^0)$.

The second-order term in the Boltzmann equation is

$$\sum_{\mathbf{k}'\sigma'}\left[P_{\mathbf{k}'\mathbf{k}}^{\sigma'\sigma\,(1)}\left(g_{\mathbf{k}\sigma}^{(2)} - g_{\mathbf{k}'\sigma'}^{(2)}\right) - P_{\mathbf{k}'\mathbf{k}}^{\sigma'\sigma\,(2)}\left(g_{\mathbf{k}\sigma}^{(1)} + g_{\mathbf{k}'\sigma'}^{(1)}\right)\right] = 0. \tag{42}$$

Making use of equations (32), (33) and (40), the solution of the second-order (*skew scattering*) term becomes

$$g_{\mathbf{k}\sigma}^{(2)} = -\alpha_H^{SS}\tau_{tr}\frac{\partial f_0(\xi_{\mathbf{k}})}{\xi_{\mathbf{k}}}(\boldsymbol{\sigma}_{\sigma\sigma}\times\mathbf{v}_{\mathbf{k}})\cdot\nabla\mu_N^{\sigma}(\mathbf{r}), \tag{43}$$

where α_H^{SS} is the dimensionless parameter of skew scattering

$$\alpha_H^{SS} = (2\pi/3)\bar{\eta}_{so}N(0)V_{imp}. \tag{44}$$

4.2. Spin and charge currents induced by SHE

Using the solutions of the Boltzmann equation given in the preceding sections, the distribution function becomes

$$f_{\mathbf{k}\sigma} \approx f_0(\xi_{\mathbf{k}}) - \sigma\frac{\partial f_0(\xi_{\mathbf{k}})}{\partial\xi_{\mathbf{k}}}\delta\mu_N(\mathbf{r}) + \tau_{tr}\frac{\partial f_0(\xi_{\mathbf{k}})}{\partial\xi_{\mathbf{k}}} \times\left[\mathbf{v}_{\mathbf{k}} - \alpha_H^{SS}\boldsymbol{\sigma}_{\sigma\sigma}\times\mathbf{v}_{\mathbf{k}}\right]\cdot\nabla\mu_N^{\sigma}(\mathbf{r}), \tag{45}$$

from which the spin and charge currents in equation (29) are calculated as $\mathbf{J}_s' = \mathbf{j}_s + \alpha_H^{SS}[\hat{\mathbf{z}}\times\mathbf{j}_q]$ and $\mathbf{J}_q' = \mathbf{j}_q + \alpha_H^{SS}[\hat{\mathbf{z}}\times\mathbf{j}_s]$, where $\hat{\mathbf{z}}$ is the polarization vector and the second terms are, respectively, the Hall spin and charge currents induced by the charge and spin currents:

$$\mathbf{j}_s = -\frac{\sigma_N}{e}\nabla\delta\mu_N, \tag{46}$$

$$\mathbf{j}_q = \sigma_N\mathbf{E}, \tag{47}$$

where $\sigma_N = 2e^2N(0)D$ is the electrical conductivity and $\delta\mu_N = \frac{1}{2}(\mu_N^{\uparrow} - \mu_N^{\downarrow})$ is the chemical potential shift. Therefore, the total spin and charge currents in equations (26) and (27) are written as

$$\mathbf{J}_q = \mathbf{j}_q + \alpha_H\left[\hat{\mathbf{z}}\times\mathbf{j}_s\right], \tag{48}$$

$$\mathbf{J}_s = \mathbf{j}_s + \alpha_H\left[\hat{\mathbf{z}}\times\mathbf{j}_q\right], \tag{49}$$

where $\alpha_H = \alpha_H^{SJ} + \alpha_H^{SS} = \bar{\eta}_{so}[1/(k_Fl) + (2\pi/3)N(0)V_{imp}]$. Equations (48) and (49) indicate that the spin current $\mathbf{j}_s$ induces the transverse charge current $\mathbf{j}_q^H = \alpha_H[\hat{\mathbf{z}}\times\mathbf{j}_s]$, while the charge current $\mathbf{j}_q$ induces the transverse spin current $\mathbf{j}_s^H = \alpha_H[\hat{\mathbf{z}}\times\mathbf{j}_q]$, as shown in figure 4.

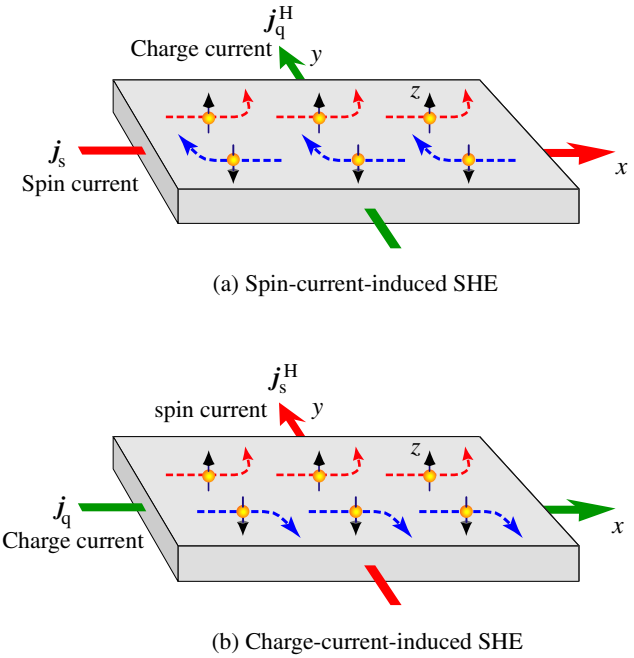

(a) Spin-current-induced SHE

(b) Charge-current-induced SHE

Figure 4. (a) Spin-current-induced SHE in which the spin current $\mathbf{j}_s$ flowing along the x-direction with the polarization parallel to the z-axis induces the charge current $\mathbf{j}_q^H$ in the y-direction. (b) Charge-current-induced SHE in which the charge current $\mathbf{j}_q$ along the x-direction induces the spin current $\mathbf{j}_s^H$ in the y-direction with the polarization parallel to the z-axis.

The spin Hall conductivity $\sigma_H = \sigma_H^{SJ} + \sigma_H^{SS}$ has the side-jump contribution $\sigma_H^{SJ} = \alpha_H^{SJ}\sigma_N$ and the skew-scattering contribution $\sigma_H^{SS} = \alpha_H^{SS}\sigma_N$, which are given by

$$\sigma_H^{SJ} = \frac{e^2}{\hbar}\eta_{so}n_e = \frac{2}{3\pi}\frac{e^2}{h}k_F\bar{\eta}_{so}, \tag{50}$$

$$\sigma_H^{SS} = \left[\frac{2\pi}{3}k_FlN(0)V_{imp}\right]\sigma_H^{SJ}, \tag{51}$$

with $n_e \sim N(0)\varepsilon_F$ being the carrier (electron) density. We note that the side-jump conductivity σ_H^{SJ} is independent of the impurity concentration. The spin Hall conductivity is dominated by skew-scattering for $(k_Fl)|N(0)V_{imp}| \gg 1$ and by side jump for $(k_Fl)|N(0)V_{imp}| \ll 1$. The spin Hall resistivity $\rho_H \approx \sigma_H/\sigma_N^2$ has linear and quadratic terms in ρ_N representing the contributions from side-jump and skew scatterings, respectively:

$$\rho_H = a_{SS}\rho_N + b_{SJ}\rho_N^2, \tag{52}$$

where $a_{SS} = (2\pi/3)\bar{\eta}_{so}N(0)V_{imp}$ and $b_{SJ} = (2/3\pi)\bar{\eta}_{so}(e^2/h)k_F$.

4.3. Spin–orbit coupling parameter

It is worthwhile to note that, if one multiplies the resistivity ρ_N and spin diffusion length λ_N, one obtains [54, 61, 81]:

$$\rho_N\lambda_N = \frac{\sqrt{3}\pi}{2}\frac{R_K}{k_F^2}\sqrt{\frac{\tau_{sf}}{\tau_{tr}}} = \frac{3\sqrt{3}\pi}{4}\frac{R_K}{k_F^2}\frac{1}{\bar{\eta}_{so}}, \tag{53}$$

Table 1. Spin–orbit coupling parameter $\bar{\eta}_{so}$ for Cu, Al, Ag, Au and Pt. Here, we use the following Fermi momenta: $k_F = 1.75 \times 10^8\,\mathrm{cm}^{-1}$ (Al), $1.36 \times 10^8\,\mathrm{cm}^{-1}$ (Cu), $1.20 \times 10^8\,\mathrm{cm}^{-1}$ (Ag) and $1.21 \times 10^8\,\mathrm{cm}^{-1}$ (Au) [82]. (We assume $1 \times 10^8\,\mathrm{cm}^{-1}$ for Pt.)

	λ_N (nm)	ρ_N ($\mu\Omega$ cm)	τ_{sf}/τ_{tr}	$\bar{\eta}_{so}$	Reference
Al	650	5.90	2.8×10^4	0.009	[10]
Al	455	9.53	3.6×10^4	0.008	[63]
Al	705	5.88	3.3×10^4	0.008	[63]
Cu	1000	1.43	1.4×10^3	0.040	[9]
Cu	1500	1.00	1.6×10^3	0.037	[47]
Cu	546	3.44	2.4×10^3	0.030	[18]
Ag	162	4.00	1.8×10^2	0.113	[19]
Ag	195	3.50	2.0×10^2	0.107	[19]
Au	168	4.00	2.0×10^2	0.107	[20]
Pt	14	12.8	6.5	0.59	[83]

where $R_K = h/e^2 \sim 25.8\,\mathrm{k}\Omega$ is the quantum resistance. Equation (53) implies that $\rho_N\lambda_N$ is expressed in terms of the spin–orbit coupling parameter $\bar{\eta}_{so}$, and provides a new method of evaluating the spin–orbit coupling in nonmagnetic metals. Using the experimental data of ρ_N and λ_N for Al, Cu, Ag and Au in equation (53), we obtain the values of the spin–orbit coupling parameter $\bar{\eta}_{so}$ in those metals, as listed in table 1. We note that the values of $\bar{\eta}_{so}$ estimated by the spin injection method are 10^2–10^3 times the value of $\bar{\eta}_{so} = \hbar^2 k_F^2/4m^2c^2 = (v_F/2c)^2$ in the free-electron model.

4.4. Nonlocal SHE

Let us consider the nonlocal spin Hall device shown in figure 5 [54, 61, 81, 84]. The magnetization of the ferromagnet (F) points in the z-direction perpendicular to the plane. Spin injection is induced by sending the current I from F to the left end of N, while the Hall voltage (V_H) is measured by the Hall bars at distance L, where charge current $\mathbf{j}_q$ is absent and only spin current $\mathbf{j}_s$ flows in the x-direction. Therefore, from equations (48) and (49), $\mathbf{J}_s = \mathbf{j}_s$ and

$$\mathbf{J}_q = \alpha_H \left[\hat{\mathbf{z}} \times \mathbf{j}_s\right] + \sigma_N \mathbf{E}, \tag{54}$$

where the first term is the Hall current induced by the spin current, and the second term is the ohmic current that builds up in the transverse direction as opposed to the Hall current. In an open circuit condition in the transverse direction, the y-component of $\mathbf{J}_q$ in equatiion (54) vanishes, which yields the relation between the Hall electric field E_y and the spin current $\mathbf{j}_s = (j_s, 0, 0)$,

$$E_y = -\alpha_H \rho_N j_s, \tag{55}$$

which is integrated with respect to y to yield the Hall voltage

$$V_H = \alpha_H w_N \rho_N j_s, \tag{56}$$

where w_N is the width of N. The spin current j_s at $x = L$ is given by

$$j_s \approx \tfrac{1}{2} P_{eff} (I/A_N) e^{-L/\lambda_N}, \tag{57}$$

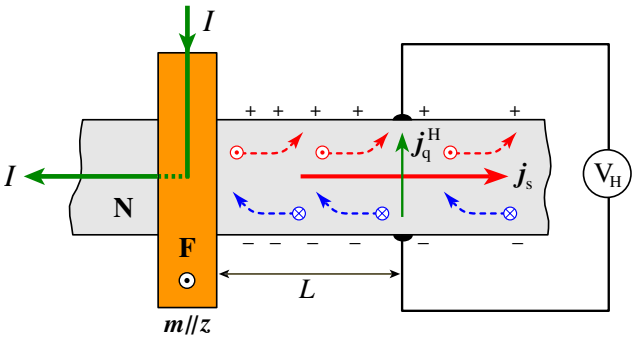

Figure 5. Nonlocal spin Hall device. The magnetization of F is pointed perpendicular to the plane. The nonlocal Hall voltage V_H is generated in the transverse direction by injecting pure spin current.

where P_{eff} is the effective spin polarization and has the tunnel spin polarization P_T for a tunnel junction and $P_{eff} = [p_F/(1 - p_F^2)](R_F/R_N)$ for a metallic contact junction. Therefore, the nonlocal Hall resistance $R_H = V_H/I$ becomes [54, 61, 81, 84]

$$\Delta R_H = \tfrac{1}{2} P_{eff} \alpha_H \frac{\rho_N}{d_N} e^{-L/\lambda_N} \tag{58}$$

with the spin-Hall angle

$$\alpha_H = \bar{\eta}_{so} \left[1/k_F l + (2\pi/3) N(0) V_{imp}\right]. \tag{59}$$

For typical values of device parameters ($P_{eff} \sim 0.3$, $d_N \sim 10\,\mathrm{nm}$ and $\rho_N \sim 5\,\mu\Omega\,\mathrm{cm}$), and $\alpha_H \sim 0.01$–0.0001 for $\bar{\eta}_{so} = 0.1$–0.01 (table 1), $k_F l \sim 100$ and $V_{imp} N(0) \sim 0.1$–0.01, the expected value of ΔR_H at $L = \lambda_N/2$ is of the order of 0.05–5 mΩ, indicating that SHE is measurable using nonlocal Hall devices.

Recently, the SHE was observed by the nonlocal spin injection technique in CoFe/Al [63, 85] under high magnetic fields perpendicular to the device plane, in Py/Cu/Pt [64, 65] using strong spin absorption by Pt, in FePt/Au [66] using a perpendicularly magnetized FePt, and in a Py/Pt bilayer by a ferromagnetic resonance (FMR) technique [67].

4.5. SHE in superconductors

SHE in a superconductor is an interesting problem for the following reasons. The spin current carried by quasiparticles (QPs) in a superconductor (SC) is deflected by spin–orbit impurity scattering and accumulate QP charge (charge imbalance) in the transverse direction. The QP charge accumulation is compensated by the Cooper pair charge owing to the overall charge neutrality, thereby creating the electric potential necessary to maintain the ECP of pairs constant in space (otherwise the pairs are accelerated). This spin and charge coupling leads to SHE in SCs [60].

In a nonlocal spin Hall device, in which N is replaced by SC as in figure 5, the nonlocal Hall voltage is greatly enhanced below the superconducting critical temperature T_c. In the superconducting state, QPs injected above the superconducting energy gap Δ carry the spin current in SC, which induces SHE. When the Hall voltage V_H is detected by

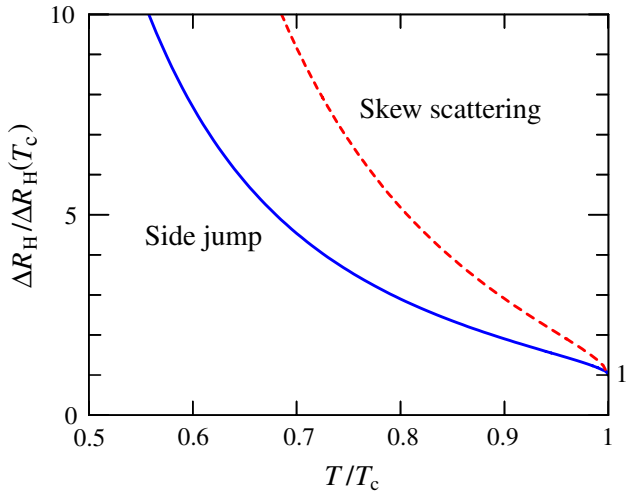

Figure 6. Temperature dependence of the nonlocal spin Hall resistance normalized to that at $T = T_c$. The solid curve indicates the side jump contribution and the dashed curve the skew scattering contribution.

Hall bars of a normal metal, the nonlocal Hall resistance is calculated as [60]

$$\Delta R_H = \frac{1}{2} P_T \frac{\rho_N}{d_N} \left(\frac{\alpha_H^{SJ}}{2 f_0(\Delta)} + \frac{\bar{\chi}_s(T)}{[2 f_0(\Delta)]^2} \alpha_H^{SS} \right) e^{-L/\lambda_N}, \quad (60)$$

where $f_0(\Delta)$ is the Fermi function at the gap energy Δ and $\bar{\chi}_s(T)$ is the spin susceptibility normalized to the normal-state one at T_c:

$$\bar{\chi}_s(T) = 2 \int_\Delta^\infty dE \frac{E}{\sqrt{E^2 - \Delta^2}} \left[-\frac{\partial f_0(E)}{\partial E} \right], \quad (61)$$

which has $\bar{\chi}_s(T) \sim 1 - [7\zeta(3)/4\pi^2](\Delta/k_B T)^2$ near T_c and $\bar{\chi}_s(T) \sim (\pi\Delta/2k_B T)^{1/2} \exp[-\Delta/k_B T]$ well below T_c. In equation (60), λ_N is unchanged in the superconducting state [86]. Figure 6 shows the temperature dependence of the spin Hall resistivity ΔR_H for quasiparticles. The solid and dashed curves indicate the SHEs due to the side-jump and skew-scattering contributions, respectively. The rapid increase of ΔR_H below T_c reflects the strong T-dependence of spin and charge imbalance of QPs in a superconductor.

5. Summary

In this article, we discussed a variety of spin transport phenomena caused by spin injection from ferromagnets into normal metals in nanostructured devices, and clarified the conditions under which efficient spin injection, accumulation and transport are realized in these devices. Using the nonlocal spin injection, a pure spin current is created in nonmagnetic conductors, so that we have the opportunity to observe the spin-current induced SHE in nonmagnetic conductors (N) via the spin–orbit scattering by nonmagnetic impurities. The observation of the SHE provides direct verification of the existence of spin current flowing in N. In a reversible way, the electrical current creates the spin current via the SHE, which provides a spin-generating source without the need to use ferromagnetic materials. The nonlocal spin injection also makes it possible to realize a nonlocal spin manipulation, in which a small ferromagnet is attached to the N and its magnetization direction is switched by the spin transfer torque due to nonlocal spin-current absorption. The advantages of nonlocal lateral structures are flexibility of the layout and the relative ease of fabricating multiterminal devices with different functionalities. The development of nonlocal spin devices is a new challenge in the research field of spin electronics.

Acknowledgments

We thank M Ichimura, H Imamura, T Kimura, Y Otani, H Seki, S Mitani, K Takanashi and E Saitoh for helpful discussions and their collaboration. This work was supported by MEXT, and the Next Generation Supercomputer Project of MEXT, Japan.

References

[1] Maekawa S and Shinjo T (eds) 2002 *Spin Dependent Transport in Magnetic Nanostructures* (London: Taylor and Francis)
[2] Maekawa S (ed) 2006 *Concepts in Spin Electronics* (Oxford: Oxford University Press)
[3] Kronmuller H and Parkin S (eds) 2007 *Handbook of Magnetism and Advanced Magnetic Materials* vols 1–5 (New York: Wiley)
[4] Žutić I, Fabian J and Das Sarma S 2004 *Rev. Mod. Phys.* **76** 323
[5] Johnson M and Silsbee R H 1985 *Phys. Rev. Lett.* **55** 1790
[6] Johnson M and Silsbee R H 1988 *Phys. Rev.* B **37** 5326
[7] Johnson M 1993 *Phys. Rev. Lett.* **70** 2142
[8] Johnson M J 1994 *Appl. Phys.* **75** 6714
[9] Jedema F J, Filip A T and van Wees B J 2001 *Nature* **410** 345
[10] Jedema F J, Heersche H B, Filip A T, Baselmans J J A and van Wees B J 2002 *Nature* **416** 713
[11] Zaffalon M and van Wees B J 2003 *Phys. Rev. Lett.* **91** 186601
[12] Urech M, Johansson J, Korenivski V and Haviland D B 2004 *J. Magn. Magn. Mater.* **272-276** e1469
[13] Kimura T, Hamrle J, Otani Y, Tsukagoshi K and Aoyagi Y 2004 *Appl. Phys. Lett.* **85** 3501
Kimura T, Hamrle J, Otani Y, Tsukagoshi K and Aoyagi Y 2004 *Appl. Phys. Lett.* **85** 3795
[14] Kimura T, Hamrle J and Otani Y 2005 *Phys. Rev.* B **72** 14461
[15] Ji Y, Hoffmann A, Jiang J S and Bader S D 2004 *Appl. Phys. Lett.* **85** 6218
[16] Miura K, Ono T, Nasu S, Okuno T, Mibu K and Shinjo T 2005 *J. Magn. Magn. Mater.* **286** 142
[17] Kimura T, Hamrle J, Otani Y, Tsukagoshi K and Aoyagi Y 2005 *J. Magn. Magn. Mater.* **286** 88
[18] Garzon S, Žutić I and Webb R A 2005 *Phys. Rev. Lett.* **94** 176601
[19] Godfrey R and Johnson M 2006 *Phys. Rev. Lett.* **96** 136601
[20] Ku J H, Chang J, Kim H and Eom J 2006 *Appl. Phys. Lett.* **88** 172510
[21] Kimura T, Otani Y and Levy P M 2007 *Phys. Rev. Lett.* **99** 166601
[22] Kimura T and Otani Y 2007 *Phys. Rev. Lett.* **99** 196604
[23] Tombros N, Jozsa C, Popinciuc M, Jonkman H T and van Wees B J 2007 *Nature* **448** 571
[24] Ohishi M, Shiraishi M, Nouchi R, Nozaki T, Shinjo T and Suzuki Y 2007 *Japan J. Appl. Phys.* **46** L605

[25] Lou X, Adelmann C, Crooker S A, Garlid E S, Zhang J, Reddy K S M, Flexner S D, Palmstrom C J and Crowell P A 2007 *Nat. Phys.* **3** 197
[26] van Son P C, van Kempen H and Wyder P 1987 *Phys. Rev. Lett.* **58** 2271
[27] Valet T and Fert A 1993 *Phys. Rev.* B **48** 7099
[28] Fert A and Lee S F 1996 *Phys. Rev.* B **53** 6554
[29] Hershfield S and Zhao H L 1997 *Phys. Rev.* B **56** 3296
[30] Takahashi S and Maekawa S 2003 *Phys. Rev.* B **67** 052409
[31] Johnson M and Byers J 2003 *Phys. Rev.* B **67** 125112
[32] Bass J and Pratt Jr W P 2007 *J. Phys.: Condens. Matter* **19** 183201
[33] van de Veerdonk R J M, Nowak J, Meservey R, Moodera J S and de Jonge W J M 1997 *Appl. Phys. Lett.* **71** 2839
[34] Ichimura M, Takahashi S, Ito K and Maekawa S 2004 *J. Appl. Phys.* **95** 7225
[35] Hamrle J, Kimura T, Yang T and Otani Y 2005 *Phys. Rev.* B **71** 094434
[36] Soulen Jr R J *et al* 1998 *Science* **282** 85
[37] Meservey R and Tedrow P M 1994 *Phys. Rep.* **238** 173
[38] Moodera J S and Mathon G 1999 *J. Magn. Magn. Mater.* **200** 248
[39] Monsma D J and Parkin S S P 2000 *Appl. Phys. Lett.* **77** 720
[40] Parkin S S P, Kaiser C, Panchula A, Rice P M, Hughes B, Samant M and Yang S-H 2004 *Nat. Mater.* **3** 862
[41] Yuasa S, Nagahama T, Fukushima A, Suzuki Y and Ando K 2004 *Nat. Mater.* **3** 868
[42] Rashba E I 2000 *Phys. Rev.* B **62** 16267(R)
[43] Fert A and Jaffrès H 2001 *Phys. Rev.* B **64** 184420
[44] Schmidt G, Richter G, Grabs P, Gould C, Ferrand D and Molenkamp L W 2000 *Phys. Rev.* B **62** 4790
[45] Johnson M 2002 *Nature* **416** 809
Jedema F J, Filip A T and van Wees B J 2002 *Nature* **416** 810
[46] Garzon S 2005 *PhD Thesis* University of Maryland
[47] Kimura T, Hamrle J and Otani Y 2005 *J. Magn. Soc. Japan* **29** 192
[48] Urech M, Johansson J, Poli N, Korenivski V and Haviland D B 2006 *J. Appl. Phys.* **99** 08M513
[49] Miura K, Kasai S, Kobayashi K and Ono T 2006 *Japan J. Appl. Phys.* **45** 2888
[50] Slonczewski J C 1996 *J. Magn. Magn. Mater.* **159** L1
[51] Berger L 1996 *Phys. Rev.* B **54** 9353
[52] Katine J A, Albert F J, Buhrman R A, Myers E B and Ralph D C 2000 *Phys. Rev. Lett.* **84** 3149
[53] Maekawa S, Inomata K and Takahashi S 2006 *Japan Patent No.* 3818276 (23 June 2006)
[54] Takahashi S and Maekawa S 2006 *Physica* C **437–438** 309
[55] Kimura T, Otani Y and Hamrle J 2006 *Phys. Rev. Lett.* **96** 037201
[56] Chien C L and Westgate C R (eds) 1980 *The Hall Effect and its Applications* (New York: Plenum)
[57] D'yakonov M I and Perel' V I 1971 *Phys. Lett.* A **35** 459
[58] Hirsch J E 1999 *Phys. Rev. Lett.* **83** 1834
[59] Zhang S 2001 *Phys. Rev. Lett.* **85** 393
[60] Takahashi S and Maekawa S 2002 *Phys. Rev. Lett.* **88** 116601
[61] Takahashi S, Imamura H and Maekawa S 2006 *Concept in Spin Electronics* Maekawa S (ed) (Oxford: Oxford University Press) Chapter 8
[62] Shchelushkin R V and Brataas A 2005 *Phys. Rev.* B **71** 045123
[63] Valenzuela S O and Tinkham M 2006 *Nature* **442** 176
[64] Kimura T, Otani Y, Sato T, Takahashi S and Maekawa S 2007 *Phys. Rev. Lett.* **98** 156601
[65] Vila L, Kimura T and Otani Y 2007 *Phys. Rev. Lett.* **99** 226604
[66] Seki T, Hasegawa Y, Mitani S, Takahashi S, Imamura H, Maekawa S, Nitta J and Takanashi K to be published
[67] Saitoh H, Ueda M, Miyajima H and Tatara G 2006 *Appl. Phys. Lett.* **88** 182509
[68] Karplus R and Luttinger J M 1954 *Phys. Rev.* **95** 1154
[69] Murakami S, Nagaosa N and Zhang S-C 2003 *Science* **301** 1348
[70] Sinova J, Culcer D, Niu Q, Sinitsyn N A, Jungwirth T and MacDonald A H 2002 *Phys. Rev. Lett.* **92** 126603
[71] Inoue J, Bauer G E W and Molenkamp L W 2004 *Phys. Rev.* B **70** 041303
[72] Kato Y K, Myers R C, Gossard A C and Awschalom D D 2004 *Science* **306** 1910
[73] Wunderlich J, Kaestner B, Sinova J and Jungwirth T 2005 *Phys. Rev. Lett.* **94** 047204
[74] Smit J 1958 *Physica* C **24** 39
[75] Berger L 1970 *Phys. Rev.* B **2** 4559
[76] Crépieux A and Bruno P 2001 *Phys. Rev.* B **64** 14416
[77] Sakurai J J and Tuan S F 1985 *Modern Quantum Mechanics* (Reading, MA: Addison-Wesley)
[78] Lyo S K and Holstein T 1972 *Phys. Rev. Lett.* **29** 423
[79] Kondo J 1964 *Prog. Theor. Phys.* **27** 772
[80] Ansermet J-P 1998 *J. Phys.: Condens. Matter* **10** 6027
[81] Takahashi S and Maekawa S 2007 *J. Magn. Magn. Mater.* **310** 2067
[82] Ashcroft N W and Mermin D 1976 *Solid State Physics* (Philadelphia, PA: Saunders College)
[83] Steenwyk S D, Hsu S Y, Loloee R, Bass J and Pratt Jr W P 1997 *J. Magn. Magn. Mater.* **170** L1
[84] Takahashi S and Maekawa S 2004 *Spin Electronics—Basic and Forefront* Inomata K (ed) (Tikyo: CMC Publishing Co., Ltd.) 28
[85] Valenzuela S O and Tinkham M 2007 *J. Appl. Phys.* **101** 09B103
[86] Yamashita T, Takahashi S, Imamura H and Maekawa S 2002 *Phys. Rev.* B **65** 172509